1

Different heating of Maxwellian and kappa distributions at shocks

Michael Gedalin [1,†] and Natalia Ganushkina[2]

[1]Department of Physics, Ben-Gurion University of the Negev, Beer-Sheva, Israel

[2]Finnish Meteorological Institute, Helsinki, Finland

Ion heating in collisionless shocks is non-adiabatic and efficient. The amount of heating
and the downstream distributions depend on the shock parameters and on the incident ion
distribution. The number of reflected ions and their distribution depend on the detailed
shape of the tail of the distribution. In supercritical shocks the reflected ion contribution
is significant. Kappa distributed ions are heated more strongly and have a larger fraction of
reflected ions than Maxwellian distributed ions with the same upstream temperature and
the same shock parameters. For kappa distributions the phase space dips are shallower.

Key words: astrophysical plasmas, space plasma physics, plasma nonlinear phenomena

1. Introduction

Shocks efficiently convert the energy of the directed flow into thermal energy (de
Hoffmann & Teller 1950). In collisionless shocks different plasma species are heated
differently (Feldman *et al.* 1982; Sckopke *et al.* 1983; Thomsen *et al.* 1985, 1987;
Schwartz *et al.* 1988; Sckopke *et al.* 1990). In an electron–proton plasma, heating occurs
at the expense of the energy of the incident ions. The incident ions cross the shock
against the cross-shock potential (Morse 1973; Formisano 1982; Schwartz *et al.* 1988;
Gedalin 1997*b*,*a*; Dimmock *et al.* 2012; Hanson *et al.* 2019) and begin to gyrate. Ion
distributions in the vicinity of the main magnetic field jump (ramp) are non-gyrotropic
(Sckopke *et al.* 1983; Burgess, Wilkinson & Schwartz 1989; Li *et al.* 1995; Gedalin
1997*a*). Farther downstream, gyrophase mixing gyrotropizes the distributions and the
gyration speeds become the dispersion in the velocity space, thus the contribution to
the ion temperature (see Gedalin (2021) and references therein). In supercritical shocks,
ion reflection comes to play a progressively more important role in ion heating with the
increase of the Mach number (Burgess *et al.* 1989; Sckopke *et al.* 1990; Zimbardo 2011;
Gedalin 2019). Reflected ions have larger gyration speeds than the ions of the bulk of the
flow and their contribution to the downstream temperature exceeds their contribution to
the downstream density. Simply put, ions may be reflected in two ways (Gedalin 2016).
Ions, which enter the ramp with sufficiently low velocities along the shock normal, are

† Email address for correspondence: gedalin@bgu.ac.il

unable to overcome the cross-shock potential and return back to the upstream region where they gyrate back to the ramp and cross it again. This mode of reflection depends mainly on the cross-shock potential and is not sensitive to the magnetic compression. Ions with sufficiently high initial velocities along the shock normal overcome the potential and cross the ramp towards the downstream region. Such ions may retain sufficiently large gyration speeds to gyrate back to the ramp. If this happens, they cross the ramp towards upstream, gyrate in the upstream region, and cross the ramp once again towards downstream. This mode requires sufficient magnetic compression to ensure that the gyration speed is larger than the drift which causes ions to proceed farther downstream. In both reflection modes magnetic deflection within the ramp affects the velocity along the shock normal, so that the above description is somewhat simplified. Ions which are reflected in both modes come from the tail of the distribution function and not from the core. Thus, the shape of the upstream distribution function may affect the downstream ion distributions and heating in supercritical shocks. Most of heating analyses, including numerical simulation, performed so far, assumed Maxwellian distribution for incident ions. However, the actual distribution of ions in the solar wind may differ and is often found to be better described as a kappa (κ) distribution (see, e.g. Nicolaou *et al.* (2018), and references therein). Since the Maxwellian and κ distributions have different tails, one may expect to observe differences in the ion distributions formed at the shock crossing, even if the velocity dispersion is the same. The objective of the present paper is to analyse the effects of the shape of the tails of these two distributions on the ion heating at a slightly supercritical shock.

2. Approach: numerical ion tracing

Since we are interested in separating the effects of the distribution from all other effects, it is reasonable to control all other shock parameters. It is most efficiently done by tracing ions as test particles across a model shock. A slightly supercritical shock is expected to be a nearly planar and stationary low-Mach number shock, with a weak overshoot. Let subscripts u and d denote upstream and downstream, respectively. We choose the coordinates so that x is along the shock normal, pointing towards downstream, and x–z is the coplanarity plane. The magnetic field profile is described as follows:

$$B_z = B_u \sin\theta \left(\frac{R-1}{2} + \frac{R+1}{2} \tanh\frac{3x}{D} \right), \tag{2.1}$$

where B_u is the upstream magnetic field magnitude, θ is the angle between the shock normal and the upstream magnetic field vector, and the magnetic compression is

$$\frac{B_d}{B_u} = \sqrt{R^2 \sin^2\theta + \cos^2\theta}. \tag{2.2}$$

The parameter D gives the shock width. We do not include any overshoot in this analysis, since its influence is expected to be minor. The upstream proton gyrofrequency is $\Omega_u = eB_u/m_p c$. The upstream proton plasma frequency is $\omega_p = \sqrt{4\pi e^2 n_u/m_p}$, where n_u is the upstream proton number density. The ion inertial length is c/ω_p and the Alfvén speed is $v_A = c\Omega_u/\omega_p$. Let the upstream plasma velocity along the shock normal in the shock frame be V_u, then the Alfvénic Mach number is $M = V_u/v_A$. The upstream convective proton gyroradius is $\rho_p = V_u/\Omega_u = M(c/\omega_p)$. In what follows we shall use dimensional parameters and variables as follows:

$$\frac{x}{\rho_p} \to x, \quad \Omega_u t \to t, \quad \frac{\boldsymbol{v}}{V_u} \to \boldsymbol{v}, \quad \frac{\boldsymbol{B}}{B_u} \to \boldsymbol{B}. \tag{2.3a–d}$$

The two most convenient shock frames and the de Hoffman–Teller frame (HT), in which the upstream and downstream plasma velocities are along the upstream and downstream magnetic field vectors, respectively, and the normal incidence frame (NIF), in which the upstream plasma velocity is along the shock normal. In HT the motional electric field $E_y(\text{HT}) = 0$ vanishes identically, while in NIF it is constant $E_y^{(\text{NIF})} = V_u B_u \sin\theta/c$ throughout the shock. In both frames $E_z = 0$. The shape of the cross-shock electric field $E_x^{(\text{HT})}$ is chosen as follows:

$$E_x^{(\text{HT})} = -K_E \frac{\text{d}B_z}{\text{d}x}, \tag{2.4}$$

where the coefficient K_E is determined from the cross-shock potential

$$\phi_{\text{HT}} = -\int_{-\infty}^{\infty} E_x \, \text{d}x \tag{2.5}$$

and is one of the model parameters. In the dimensionless form we have

$$s_{\text{HT}} = e\phi_{\text{HT}}/(m_p V_u^2/2). \tag{2.6}$$

The non-coplanar magnetic field is chosen in a similar form,

$$B_y = K_B \frac{\text{d}B_z}{\text{d}x}, \tag{2.7}$$

while

$$\phi_{\text{NIF}} - \phi_{\text{HT}} = \frac{V_u \tan\theta}{c} \int_{-\infty}^{\infty} B_y \, \text{d}x. \tag{2.8}$$

For $V_u/\cos\theta \ll c$ the transformation between the two frames is non-relativistic which means that the magnetic field can be considered the same. The parameter

$$s_{\text{NIF}} = e\phi_{\text{NIF}}/(m_p V_u^2/2) \tag{2.9}$$

is also the model parameter which determines the coefficient K_B. In the present analysis $s_{\text{NIF}} = 0.4$, $s_{\text{HT}} = 0.1$ and $D = (c/\omega_p)$. The chosen magnetic compression is $B_d/B_u = 2.6$ and $\theta = 70°$. The Mach number $M = 2.9$ is derived from isotropic Rankine–Hugoniot relations (Kennel 1988) with $\beta_p = 8\pi n_u T_u/B_u^2 = 0.2$. Here T_u is the upstream ion temperature.

The initial upstream distributions of ions are taken either Maxwellian

$$f_u^{(M)}(\boldsymbol{v}) = \frac{n_u}{(2\pi)^{3/2} v_T^3} \exp\left(-\frac{(\boldsymbol{v} - \boldsymbol{V})^2}{2v_T^2}\right) \tag{2.10}$$

or a κ distribution

$$f_u^{(K)}(\boldsymbol{v}) = \frac{n_u}{\pi^{3/2} v_T^3} \left(\kappa - \frac{3}{2}\right)^{-3/2} \frac{\Gamma(\kappa + 1)}{\Gamma(\kappa - 1/2)} \left(1 + \frac{(\boldsymbol{v} - \boldsymbol{V})^2}{(2\kappa - 3)v_T^2}\right)^{-\kappa - 1}, \tag{2.11}$$

where in both cases

$$n_u \boldsymbol{V} = \int f_u(\boldsymbol{v}) \, \text{d}^3\boldsymbol{v}, \tag{2.12}$$

$$n_u v_T^2 = \int (\boldsymbol{v} - \boldsymbol{V})^2 f_u(\boldsymbol{v}) \, \text{d}^3\boldsymbol{v} \tag{2.13}$$

and Γ is the Γ-function. In the present analysis $\kappa = 4$ (Smith *et al.* 2022).
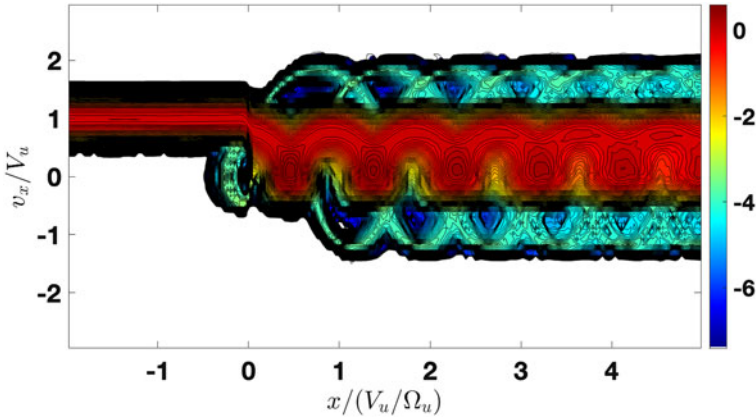
FIGURE 1. The upstream (left-hand side) and downstream (right-hand side) gyrotropic distributions for initially Maxwellian distributed ions, on a log scale.

3. Downstream distributions and heating parameters

Figure 1 shows the distributions functions $f_u(v_\parallel, v_\perp)$ and $f_d(v_\parallel, v_\perp)$ for the Maxwellian distributed incident ions. Here

$$v_\parallel = \frac{\boldsymbol{v} \cdot \boldsymbol{B}}{|\boldsymbol{B}|}, \tag{3.1}$$

$$v_\perp = \frac{|(\boldsymbol{v} - \boldsymbol{V}) \times \boldsymbol{B}|}{|\boldsymbol{B}|}, \tag{3.2}$$

where $\boldsymbol{B}$ is the local magnetic field. The upstream distributions are gyrotropic by choice. The downstream distributions become gyrotropic well beyond the shock transition. The distributions are in HT. The maximum of the downstream distribution is not at $v_\perp = 0$ which shows that initially the whole distribution gyrates around the magnetic field. After gyrotropization, this gyration is the main contribution to the velocity dispersion, that is, to the temperature. There is a distinct population of reflected ions. Their density is low and there is a clear gap between the directly transmitted ions and reflected ions. The figure uses a logarithmic scale with $f_{\min}/f_{\max} > 10^{-6}$. The upstream temperature of the ions is $T_u/m_p V_u^2 = 0.0118$. The downstream parallel temperature is $T_{d,l} = T_u$, while the downstream perpendicular temperature is $T_{d,p}/m_p V_u^2 = 0.0973$.

Figure 2 shows the distributions functions $f_u(v_\parallel, v_\perp)$ and $f_d(v_\parallel, v_\perp)$ in the same format as in figure 1. The population of the reflected ions is substantially larger, and there is no gap between the directly transmitted and reflected ions. The upstream temperature of the ions is $T_u/m_p V_u^2 = 0.0118$, as for the Maxwellian ions. The downstream parallel temperature is $T_{d,l}/m_p V_u^2 = 0.0126$, while the downstream perpendicular temperature is $T_{d,p}/m_p V_u^2 = 0.1004$. The 10 % difference in the downstream perpendicular temperature is due to the reflected ions. The difference in the downstream density is negligible.

Figure 3 shows the downstream reduced distribution

$$f_d(v_\perp) = \int_{-\infty}^{\infty} f_d(v_\parallel, v_\perp) \, \mathrm{d}v_\parallel, \tag{3.3}$$

for the initially Maxwellian ions (blue) and initially κ ions (red). The left-hand vertical black line stands at the maximum of the distribution of the directly transmitted population.
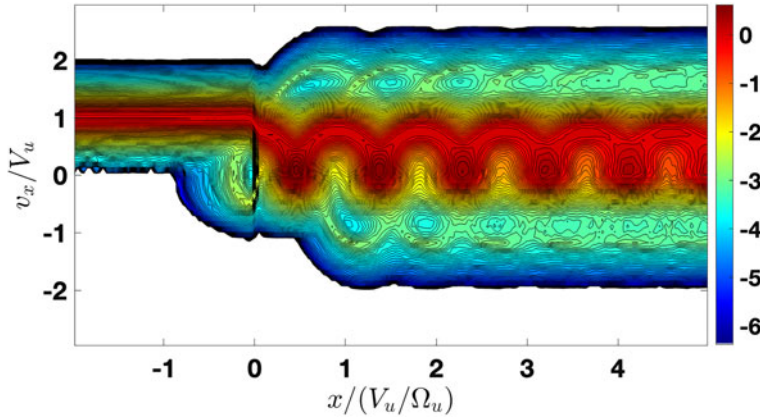
FIGURE 2. The upstream (left-hand side) and downstream (right-hand side) gyrotropic distributions for initially κ-distributed ions, on a log scale.
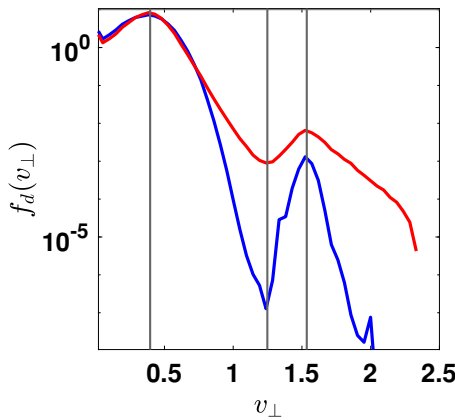
FIGURE 3. The downstream reduced distribution for the initially Maxwellian ions (blue) and initially κ ions (red). The left-hand vertical black line stands at the maximum of the distribution of the directly transmitted population. The right-hand line marks the maximum of the reflected ions. The middle line is for the minimum of the distribution.

The right-hand line marks the maximum of the reflected ions. The middle line is for the minimum of the distribution. There are no noticeable differences in the positions of the three points in both cases. For κ ions the maximum of the reflected ions and the integral under the curve part, corresponding to these ions, are substantially larger. In the minimum the distribution function does not drop as strongly as for the Maxwellian ions.

Figure 4 shows the reduced distribution function

$$f(x, v_x) = \int f(x, \boldsymbol{v}) \, \mathrm{d}v_y \, \mathrm{d}v_z \qquad (3.4)$$

throughout the shock for initially Maxwellian ions. The gyration and relaxation of directly transmitted ions is clearly seen, as well as the gyrating reflected ions. There is a phase space hole separating the two populations. Reflected ions are seen in the upstream region up to the distance $\approx 0.5(V_u/\Omega_u)$.
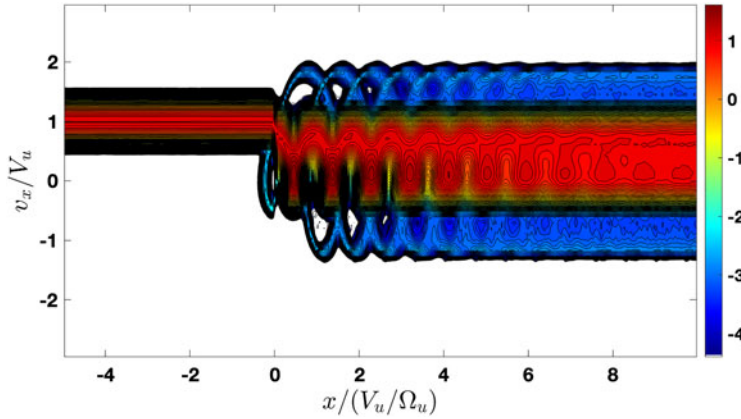
FIGURE 4. The reduced distribution function $f(x, v_x)$ throughout the shock for initially Maxwellian ions.
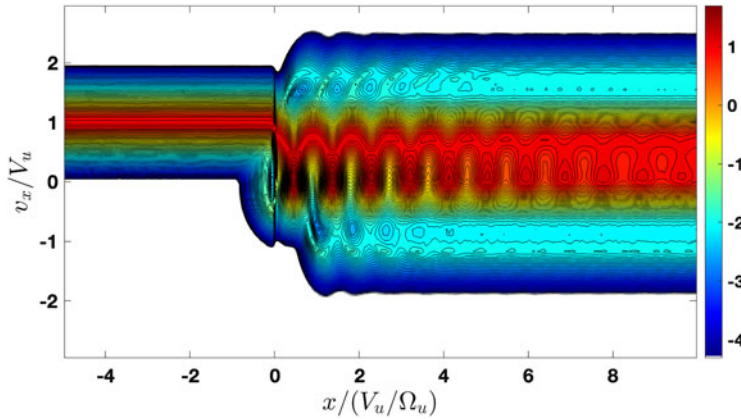
FIGURE 5. The reduced distribution function $f(x, v_x)$ throughout the shock for initially κ ions.

Figure 5 throughout the shock for initially κ ions. Now the two populations, albeit clearly seen, are not separated by phase space holes. Reflected ions are seen in the upstream region up to the distance $\approx (V_u/\Omega_u)$. However, their density there is hardly detectable in reality. The sharp drop of the distribution at $0.5(V_u/\Omega_u)$ for Maxwellian ions versus the smooth decrease over $-(V_u/\Omega_u) < x < -0.5(V_u/\Omega_u)$ is because of the much faster drop of the tail for Maxwellian ions. The slower decreasing tail of κ is also responsible for filling the phase space holes.

4. Conclusions

Longer tails of the distribution function of incident ions result in stronger heating and smaller anisotropy of the downstream distribution. Both effects are due to stronger ion reflection, since the reflected ions come from the tail of the distribution. Longer tails may be also responsible for filling the ion phase space holes. The distribution of reflected ions is much more diffuse for κ-distributed ions than for Maxwellian-distributed ions.

Acknowledgements

Funding

The work was partially supported by the European Union's Horizon 2020 research and innovation programme under grant agreement no. 101004131 (SHARP).

Declaration of interests

The authors report no conflict of interest.

REFERENCES

BURGESS, D., WILKINSON, W.P. & SCHWARTZ, S.J. 1989 Ion distributions and thermalization at perpendicular and quasi-perpendicular supercritical collisionless shocks. *J. Geophys. Res.* **94**, 8783.

DE HOFFMANN, F. & TELLER, E. 1950 Magneto-hydrodynamic shocks. *Phys. Rev.* **80** (4), 692–703.

DIMMOCK, A.P., BALIKHIN, M.A., KRASNOSELSKIKH, V.V., WALKER, S.N., BALE, S.D. & HOBARA, Y. 2012 A statistical study of the cross-shock electric potential at low Mach number, quasi-perpendicular bow shock crossings using Cluster data. *J. Geophys. Res.* **117** (A), 02210.

FELDMAN, W., BAME, S., GARY, S., GOSLING, J., MCCOMAS, D., THOMSEN, M., PASCHMANN, G., SCKOPKE, N., HOPPE, M. & RUSSELL, C. 1982 Electron heating within the Earth's bow shock. *Phys. Rev. Lett.* **49** (3), 199–201.

FORMISANO, V. 1982 Measurement of the potential drop across the Earth's collisionless bow shock. *Geophys. Res. Lett.* **9**, 1033.

GEDALIN, M. 1997a Ion dynamics and distribution at the quasiperpendicular collisionless shock front. *Surv. Geophys.* **18** (6), 541–566.

GEDALIN, M. 1997b Ion heating in oblique low-Mach number shocks. *Geophys. Res. Lett.* **24** (2), 2511–2514.

GEDALIN, M. 2016 Transmitted, reflected, quasi-reflected, and multiply reflected ions in low-Mach number shocks. *J. Geophys. Res.* **121** (1), 10.

GEDALIN, M. 2019 Kinematic collisionless relaxation of ions in supercritical shocks. *Front. Phys.* **7**, 692.

GEDALIN, M. 2021 Shock heating of directly transmitted ions. *Astrophys. J.* **912** (2), 82.

HANSON, E.L.M., AGAPITOV, O.V., MOZER, F.S., KRASNOSELSKIKH, V., BALE, S.D., AVANOV, L., KHOTYAINTSEV, Y. & GILES, B. 2019 Cross-shock potential in rippled versus planar quasi-perpendicular shocks observed by MMS. *Geophys. Res. Lett.* **46** (5), 2381–2389.

KENNEL, C.F. 1988 Shock structure in classical magnetohydrodynamics. *J. Geophys. Res.* **93** (A8), 8545–8557.

LI, X., LEWIS, H.R., LABELLE, J., PHAN, T.D. & TREUMANN, R.A. 1995 Characteristics of the ion pressure tensor in the Earth's magnetosheath. *Geophys. Res. Lett.* **22** (6), 667–670.

MORSE, D.L. 1973 Electrostatic potential rise across perpendicular shocks. *Plasma Phys.* **15** (1), 1262–1264.

NICOLAOU, G., LIVADIOTIS, G., OWEN, C.J., VERSCHAREN, D. & WICKS, R.T. 2018 Determining the kappa distributions of space plasmas from observations in a limited energy range. *Astrophys. J.* **864** (1), 3.

SCHWARTZ, S.J., THOMSEN, M.F., BAME, S.J. & STANSBERRY, J. 1988 Electron heating and the potential jump across fast mode shocks. *J. Geophys. Res.* **93** (A11), 12923–12931.

SCKOPKE, N., PASCHMANN, G., BAME, S.J., GOSLING, J.T. & RUSSELL, C.T. 1983 Evolution of ion distributions across the nearly perpendicular bow shock – specularly and non-specularly reflected-gyrating ions. *J. Geophys. Res.* **88** (A8), 6121–6136.

SCKOPKE, N., PASCHMANN, G., BRINCA, A.L., CARLSON, C.W. & LUEHR, H. 1990 Ion thermalization in quasi-perpendicular shocks involving reflected ions. *J. Geophys. Res.* **95**, 6337.

SMITH, W.P., RENFROE, K., POGORELOV, N.V., ZHANG, M., GEDALIN, M. & KIM, T. 2022 Bulk properties of pickup ions derived from the ulysses solar wind ion composition spectrometer data. *Astrophys. J.* **933**, 124.

THOMSEN, M.F., GOSLING, J.T., BAME, S.J. & MELLOTT, M.M. 1985 Ion and electron heating at collisionless shocks near the critical Mach number. *J. Geophys. Res.* **90** (A1), 137.

THOMSEN, M., STANSBERRY, J., BAME, S. & GOSLING, J. 1987 Strong electron heating at the Earth's bow shock. *J. Geophys. Res.* **92**, 10119–10124.

ZIMBARDO, G. 2011 Heavy ion reflection and heating by collisionless shocks in polar solar corona. *Planet. Space Sci.* **59** (7), 468–474.